


# Enhancement of sound by soft reflections in exponentially chirped crystals

Cite as: AIP Advances 4, 124402 (2014); <https://doi.org/10.1063/1.4902508>

Submitted: 07 October 2014 . Accepted: 12 November 2014 . Published Online: 20 November 2014

A. Cebrecos, R. Picó, V. J. Sánchez-Morcillo, K. Staliunas, V. Romero-García, and L. M. Garcia-Raffi 

## COLLECTIONS

Paper published as part of the special topic on [Chemical Physics](#), [Energy, Fluids and Plasmas](#), [Materials Science](#) and [Mathematical Physics](#)



View Online



Export Citation



CrossMark

## ARTICLES YOU MAY BE INTERESTED IN

[Enhancement of sound in chirped sonic crystals](#)

Applied Physics Letters **102**, 091906 (2013); <https://doi.org/10.1063/1.4793575>

[Asymmetric propagation using enhanced self-demodulation in a chirped phononic crystal](#)

AIP Advances **6**, 121601 (2016); <https://doi.org/10.1063/1.4968612>


[Broadband quasi perfect absorption using chirped multi-layer porous materials](#)

AIP Advances **6**, 121605 (2016); <https://doi.org/10.1063/1.4971274>



**NEW!**

Sign up for topic alerts  
New articles delivered to your inbox



## Enhancement of sound by soft reflections in exponentially chirped crystals

A. Cebrecos,<sup>1,a</sup> R. Picó,<sup>1</sup> V. J. Sánchez-Morcillo,<sup>1</sup> K. Staliunas,<sup>2</sup>  
 V. Romero-García,<sup>3</sup> and L. M. Garcia-Raffi<sup>4</sup>

<sup>1</sup>*Instituto de Investigación para la Gestión Integrada de zonas Costeras, Universitat Politècnica de València, Paranimf 1, 46730, Grao de Gandia, València, Spain*

<sup>2</sup>*ICREA, Departament de Física i Enginyeria Nuclear, Universitat Politècnica de Catalunya, Colom 11, E-08222 Terrasa, Barcelona, Spain*

<sup>3</sup>*LUNAM Université, Université du Maine, CNRS, LAUM UMR 6613, Av. O. Messiaen, 72085 Le Mans, France*

<sup>4</sup>*Instituto Universitario de Matemática Pura y Aplicada, Universidad Politécnica de Valencia, Camino de Vera s/n, 46022, Valencia, Spain*

(Received 7 October 2014; accepted 12 November 2014; published online 20 November 2014)

The enhancement of sound inside a two dimensional exponentially chirped crystal during the soft reflections of waves is experimentally and theoretically explored in this work. The control of this enhancement is achieved by a gradual variation of the dispersion in the system by means of a chirp of the lattice constant. The sound enhancement is produced at some planes of the crystal in which the wave is softly reflected due to a progressive slowing down of the sound wave. We find that the character of the sound enhancement depends on the function of the variation of dispersion, i.e., on the function of the chirp. A simple coupled mode theory is proposed to find the analytical solutions of the sound wave enhancement in the exponentially chirped crystal. Harmonic and time domain numerical simulations are performed to interpret the concept of the soft reflections, and to check the analytically calculated field distributions both in good agreement with experiments. Specially we obtain stronger sound enhancement than in linearly chirped crystals. This sound enhancement could motivate applications in energy harvesting, e.g., to increase the efficiency of detectors and absorbers. © 2014 Author(s). All article content, except where otherwise noted, is licensed under a Creative Commons Attribution 3.0 Unported License. [<http://dx.doi.org/10.1063/1.4902508>]

### I. INTRODUCTION

During the last decades, many efforts have been done to use periodic structures for the control of wave propagation. Such periodic structures, having a period of the order of the wavelength, are the so-called photonic crystals<sup>1</sup> for electromagnetic waves and the phononic crystals<sup>2</sup> for the elastic/acoustic waves. A phononic crystal consists of a periodic distribution of scatterers, whose bulk properties (i.e., elasticity and density) differ from those of the host medium. Based on their dispersion properties, many interesting effects can be observed such as the formation of band-gaps,<sup>3,4</sup> negative refraction,<sup>5</sup> birefracton,<sup>6</sup> self-collimation,<sup>7,8</sup> extraordinary transmission,<sup>9</sup> giving rise to novel devices and effects such as spatial<sup>10,11</sup> and frequency<sup>12</sup> filters, far field<sup>13</sup> and near field<sup>14</sup> focusing, or sound diodes.<sup>15</sup> Of special interest is the possibility to enhance both spatially and temporally the wave at particular locations inside the crystal, with potential applications as, for example, energy harvesting or enhanced absorption.

Different mechanisms can be used to enhance the waves inside a crystal. At low frequencies (with  $\lambda \gg a$ , being  $\lambda$  the wavelength of the incident frequency and  $a$  the distance between the scatterers, or lattice constant), Fabry-Pérot resonances can enhance the wave inside the structure due

<sup>a</sup>Electronic mail: [alcebrui@epsg.upv.es](mailto:alcebrui@epsg.upv.es)

to the finite thickness of the crystal,  $L$ , at frequencies related with this thickness,  $f = nc/2L$  being  $n$  an integer number. At higher frequencies, in the highly dispersive regime of the periodic structure in which  $\lambda \approx a$ , enhanced localized modes can be excited by the presence of point defects. The periodicity can be locally broken by creating the point defects producing a localized enhanced mode around the defect at a frequency inside the band gap.<sup>16,17</sup> In both cases, the low frequency and the dispersion regime, the wave can be enhanced for a set of narrow bands (modes), but no broadband enhancement is possible. On the other hand, random systems, in the regime where the wavelength of the incident wave is comparable with the size of the scatterers, present a transition from its diffusion regime to a localized regime, where enhanced localized modes appear in the structure for a broader frequency regime.<sup>18,19</sup> In this case the strong deviation from Rayleigh statistics is interpreted as a signature of Anderson localization.

Recently, some of us presented an acoustic wave propagation effect, consisting of the wave enhancement due to the progressive decrease of the group velocity along the propagation direction.<sup>20</sup> Such a progressive slowing-down of the waves was predicted and demonstrated in a two-dimensional chirped (also known as graded or adiabatic tapered) sonic crystal, a structure made of rigid scatterers embedded in air in which the lattice constant along the wave propagation direction gradually changes with a profile,  $a = a(x)$ , depending on the position,  $x$ . Sound enhancement and slowing down are two related phenomena that occur as the wave approaches to the bandgap; at this position, the waves reaches a zero group velocity and starts propagating backwards, in a process that we call a soft reflection. For particular chirp profiles, the wave can be substantially enhanced around the turning plane, whose position inside the crystal depends on the wave frequency. Chirped structures have been also used in optics<sup>21,22</sup> and acoustics<sup>23–25</sup> for different purposes such as rainbow trapping,<sup>26–28</sup> mirage formation,<sup>29</sup> the opening of wide full band gaps,<sup>23</sup> or also to control the spatial dispersion and focalizing beams in reflection.<sup>22</sup>

From a practical point of view, it is desirable to obtain the highest enhancement or wave concentration (highest intensity in a shorter distance). The previous study considered a chirped structure with a adiabatic and linear change of the period,<sup>20</sup> where a moderate enhancement was demonstrated. In this work we explore the properties of a sonic crystal with exponential one. This profile of chirp is of interest because it possess simple analytical solutions, a unique feature that shares with a linear chirp. This allows easier estimations of wave propagation properties depending on system parameters. Most importantly, the exponential chirp is shown to produce a stronger wave enhancement in comparison to the linear profile in Ref. 20. Therefore in this work we report new analytical, numerical and experimental results about a sonic crystal with exponential chirp, and compare the predictions from different methods, showing good agreement between them. Special attention is paid to the interpretation in time domain of the soft reflections produced in the crystal, which are related to the spatial enhancement of the wave in the spatial domain. Simulations are performed in harmonic and time-domain by Finite Element Method (FEM), showing very good agreement with both analytical and experimental results measured in an echo-free chamber.

## II. DISPERSION IN CHIRPED STRUCTURES AND SOFT REFLECTIONS

Dispersion curves  $\omega(k)$  in periodic structures predict very small group velocity ( $v_g = \partial\omega/\partial k$ ) of the propagating waves close to the band edges, and correspondingly a large dispersion of the incident wave packet. In chirped structures in which the lattice constant gradually varies according to a predetermined profile, the dispersion relation also evolves gradually inside the crystal following the variation of the profile along the structure. The main assumption in these structures is that the variation of the profile is so slow that each point in the chirped crystal can be characterized by a *local* dispersion relation, which is the dispersion of an infinitely extended periodic crystal with values of the parameters (lattice constant and filling fraction) at the evaluation point. As an example we show in Fig. 1(a) the evolution of the band gap in a chirped crystal with an exponential profile (inset of Fig. 1(a) shows the spatial distribution of the rigid scatterers inside the chirped crystal. See Section IV for more details about the definition of the profile  $a = a(x)$ ). In each point inside the chirped crystal we have considered a rectangular array with the local lattice constant and the local filling fraction. Then, using the plane wave expansion,<sup>17</sup> we have calculated the band structure

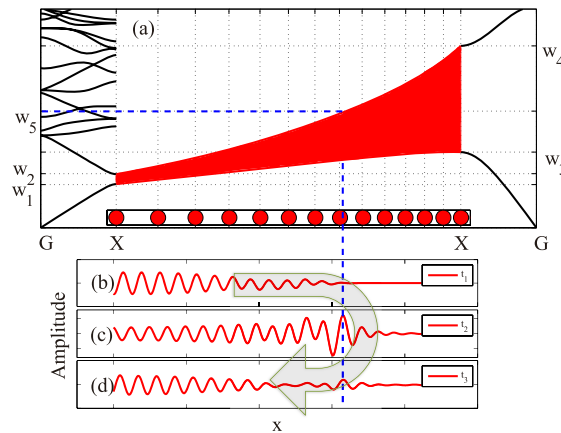


FIG. 1. (a) Local band gaps in exponential chirped structures. Left (right) panel shows the band structures at the entrance (exit) of the system calculated using plane wave expansion. Middle panel shows the evolution of the bandgap within the discrete structure. Inset shows the position of the scatterers inside the system obtained from the exponential chirped shown in Sec. IV. (b), (c) and (d) respectively show the spatial profile of a pulse evaluated at an instant  $t_1$  before the pulse reaches the turning plane, at the instant  $t_2$  when the pulse reaches the turning plane and at the instant  $t_3$  after the pulse reaches the turning plane.

in each point. The number of the plane waves considered for the calculation is enough to ensure the convergence of the plane wave expansion, in our case 1089 plane waves. In the left part, we represent the dispersion relation at the entrance of the crystal, showing the band gap in the range  $[\omega_1=1197, \omega_2=1468]$  Hz. In the central part of Fig. 1(a), we represent the evolution of the width of the first band gap in the  $\Gamma X$  direction along the chirped crystal. As the filling fraction gradually increases along the chirped crystal, the width of the band gap also gradually increases, as shown by the red area in Fig. 1(a) up to the exit of the crystal, where the width of the band gap  $[\omega_3=2073, \omega_4=4988]$  Hz corresponds to the periodicity and filling fraction at the exit of the crystal, as shown in the right part of Fig. 1(a).

In order to have propagation of waves inside the crystal, the frequency of the incident wave must belong to some of the propagating bands of the dispersion relation at the entrance of the crystal. In a general way, we consider now an incident gaussian packet centred at  $\omega_5$  which, as shown in Fig. 1(a), is in the propagating region at the entrance of the crystal. However, as  $\omega_5 < \omega_4$ , the wave will arrive to a band gap inside the crystal corresponding to a lattice constant and filling fraction that covers  $\omega_5$ . The wave entering into the crystal is gradually slowing down because, in the course of propagation, it approaches to the edges of local *local* band gap inside the crystal. At a particular depth corresponding to the band-edge, where the group velocity is zero (in absence of losses), the forward propagating wave stops, turns around, and starts propagating backwards, suffering, what we call here, a “soft” reflection. This reflection effect is observed in the temporal domain in Figs. 1(b)-(d). We show the wave packet at three different instants inside the crystal: (b) before (c) at the instant and (d) after the wave packet reaches the reflecting plane. Figure 1(c) shows how the wave enhancement in the soft reflection area.

### III. COUPLED MODE THEORY: ANALYTICAL RESULTS

We propose an analytical description of the problem of the enhancement in an exponential chirp profile, based in the so called coupled mode theory. The approach is valid under some approximations. We first notice that at frequencies close to the first band gap, an incident plane wave basically propagates along the direction of incidence (the energy flow along other transversal directions is negligible), and a one-dimensional plane wave description is justified, as shown in Ref. 20. Under such conditions, the medium is roughly equivalent to a multilayered structure, with each plane of scatterers behaving as a layer of a different material. In coupled mode theory, the bandgaps appear as a result of the resonant coupling between the forward and the backward waves.

Coupled mode theory is applicable for media with periodic modulation of the parameters, but also for a smooth chirp profile (when the period changes adiabatically) and for frequencies close to the band-gap. It is based on the following assumptions: (i) the full pressure field consists of forward and backward propagating waves,  $P = A(x)e^{ikx-i\omega t} + B(x)e^{-ikx-i\omega t}$ , with amplitudes slowly evolving in space, and (ii) the crystal is accounted as a periodic variation of the sound velocity  $c$  with the period of the crystal,  $c = c_0 + \Delta c \cos(Qx)$  where  $Q = 2\pi/a$ . Substituting in the linear wave equation and scaling the space as  $X = x/a$ , the following coupled amplitude equations system is readily obtained

$$\frac{dA}{dX} = iB e^{2i\Delta Q X}, \quad (1)$$

$$\frac{dB}{dX} = iA e^{-2i\Delta Q X}, \quad (2)$$

where  $\Delta Q = a(k - k_B)$  is the detuning from normalized Bragg resonance, with  $k_B = \pi/a(X)$ . After some manipulation, a single second order equation for the slow amplitudes can be obtained, as

$$\frac{d^2 A}{dX^2} = im(X) \frac{dA}{dX} + A, \quad (3)$$

where  $m(X) = d(\Delta q X)/dX$  is a slowly varying function of distance, related to the normalized chirp profile  $a(X)$  by a simple transformation, which vanishes at Bragg resonance  $\Delta q = 0$ . For several particular cases the above equation has analytical solutions. One case, considered in Ref. 20, corresponds to a linear chirp profile  $m(X) = \alpha(X - X_0)$ . In this case the field distribution in space is described by a Hermite function with complex index, and presents sound enhancement at planes close to Bragg resonance. We consider here the case of an exponential chirp, in the form  $m(X) = e^{bX} - 1$ . In this case an analytical solution also exists, given by

$$A(X) = e^{-bX} L_n^s \left( \frac{ie^{bX}}{b} \right), \quad (4)$$

where  $L_n^s$  is a generalized Laguerre polynomial,<sup>30</sup> with the indexes defined as  $n = (-1)^{5/6}/b$  and  $s = \sqrt{3}/b$ .

In Fig. 2 the profile of the squared amplitude of the wave (normalized intensity) is shown along the chirped structure. We consider here wave incoming from the left side. Continuous blue line represents the results from Eq. (4) for a chirp parameter  $b = -0.05$ , and green open dots represents

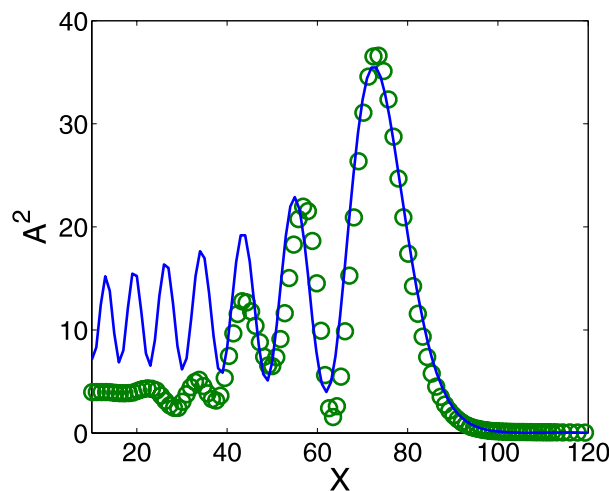


FIG. 2. Continuous line represents the amplitude profile in the exponentially chirped crystal, as given by the analytical solution of Eq. (4) calculated using  $b = -0.05$ . Green dots represents the envelope for the of the experimental case as shown also in Fig. 4(d).

the envelope of the experimental data for the case of 2700 Hz. Recall that we represent here the wave envelope, so additional field oscillations with the period of the structure are also present (not shown). The effect of the exponential variation of the lattice constant is evident. A significant enhancement of the wave amplitude appears at the end of the path of the wave (bright plane), just before the turning plane (local band gap). We notice that due to the range of validity of the model, is in the range of frequencies near the band gap in which the theory agrees well with the experiments, as expected. The region in which these oscillations become important is much smaller than in the case of linear chirp (see Fig. 5 (b) in Ref. 20) and the amplitude is more localized. This is one of the main advantages of the chirp profile with respect to the linear one.

#### IV. EXPERIMENTAL SETUP

Experimental measurements were carried out with a two-dimensional sonic crystal with rectangular local symmetry, as illustrated in Fig. 3(a). The crystal is made of acoustically rigid aluminum cylinders, with radius  $r = 2$  cm, and height  $h = 1$  m, embedded in air. The spatial period is constant in transverse-to-propagation direction  $y$ ,  $a_y = 10$  cm, whereas an exponential chirp profile is introduced for the period along the propagation direction  $x$ :  $a_n = a_0 e^{-\alpha x_{n-1}}$ , where  $a_0$  is the lattice constant at the entrance of the chirped structure,  $\alpha$  is the exponential chirp parameter and  $x_j$  the local position in direction  $x$  of the  $j$ -th layer. A chirped crystal formed by 14 rows and 6 columns is considered in this work, with  $a_0 = 12.5$  cm,  $a_{13} = 4.88$  cm, and  $\alpha = 0.01$  m<sup>-1</sup>.

We performed experiments in an echo-free chamber sized  $8 \times 6 \times 3$  m<sup>3</sup> with an automatized acquisition system, 3DReAMS (3D Robotized e-Acoustic Measurement System).<sup>16,17</sup> This system enables the measurement of pressure fields along complex trajectories as well as inside the crystals. Fig. 3(a) shows the grid of hooks used for hanging cylinders to design the chirped structure which is covered in the setup with an absorbent material to avoid additional reflections in our measurements. Fig. 3(b) shows the negative chirped crystal (decreasing lattice constant) made of Al cylinders inside the echo-free chamber (for propagation directed upwards in Fig. 3(a)) used in this work.

#### V. SPATIAL ENHANCEMENT OF THE ACOUSTIC FIELD

Sound pressure amplitude,  $|p|$ , was recorded along a line path by moving the microphone along the  $x$ -axis in the space between two rows of scatterers. The recorded amplitude has been normalized with respect to the amplitude of the incident wave,  $|p_0|$ . As a result, a two-dimensional

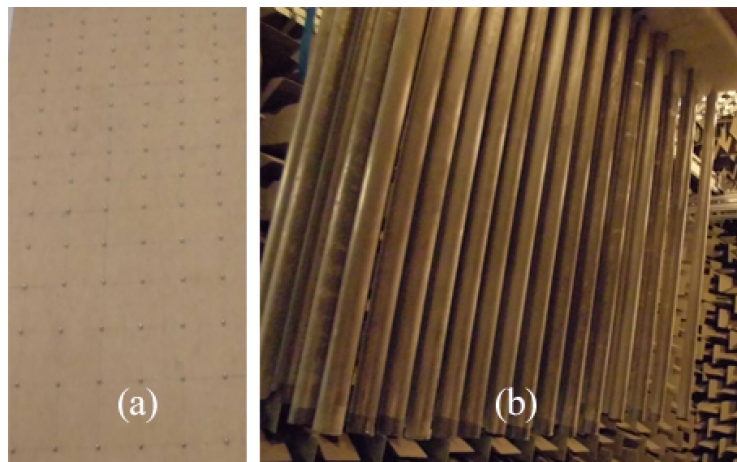


FIG. 3. Photographs of the experimental setup. (a) The grid (14 rows by 6 columns) of hanging points of the cylinders. (b) The chirped sonic crystal made of aluminium cylinders of 1 m length and 2 cm radius, hanging vertically in the anechoic chamber.



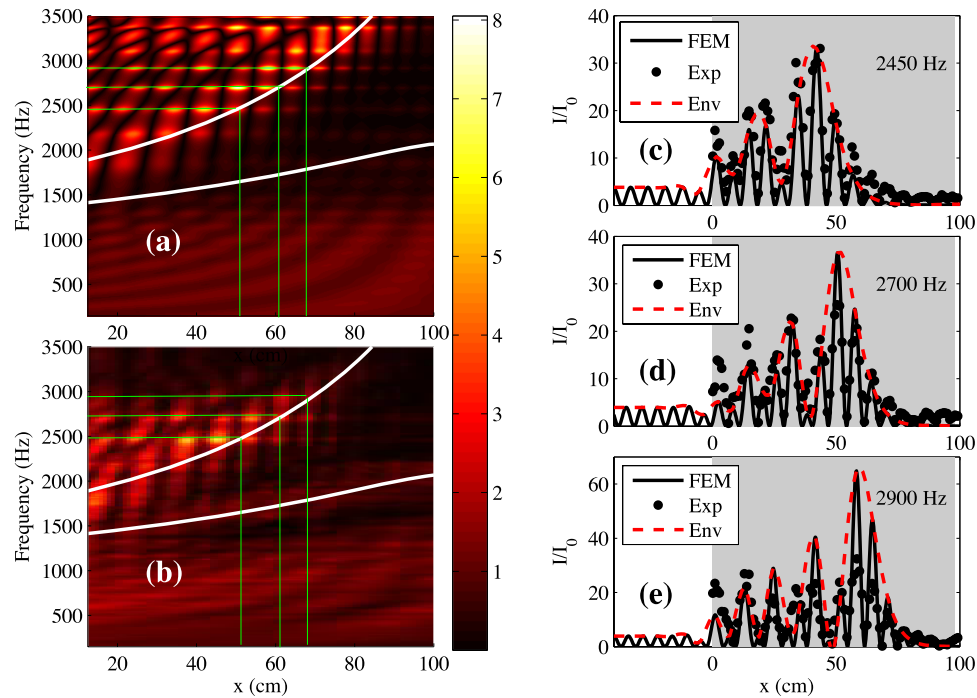


FIG. 4. (a) Numerical simulations and (b) experimental results of the normalized acoustic field with respect to the incident waves, i.e.,  $|p|/|p_0|$ , inside the chirped sonic crystal. White continuous lines define the limits of the upper and lower edges of the first band gap as the periodicity changes inside the structure. Green lines illustrate the frequencies shown in (c), (d), (e) and the corresponding positions of the turning planes inside the crystal. (c), (d) and (e) show the normalized acoustic intensity,  $I/I_0 = |p|^2/|p_0|^2$  for a longitudinal cut inside the crystal at three frequencies 2450 Hz, 2700 Hz and 2900 Hz respectively (shown also in (a) and (b)). Grey shaded rectangle denotes the area covered by the exponential chirped crystal.

frequency-space map representing the normalized acoustic field,  $|p|/|p_0|$ , inside the structure is obtained. The map shown in Fig. 4(a) is numerically calculated using FEM in harmonic analysis and Fig. 4(b) shows the normalized map directly obtained from experimental measurements. As an eye guide, we plot also in Figs. 4(a) and 4(b) the evolution of the band gap along the exponential chirped crystal (white continuous lines), obtained using plane wave expansion as described in Section II. It is worth noting here the wave enhancement at positions just before the upper band edge. We notice here that the turning planes at these frequencies appear at the positions  $x = 50$  cm,  $60$  cm and  $64.5$  cm, respectively, as numerically and experimentally shown in Figs. 4(a)-4(b). As expected, the upper edge of the local band gaps corresponds to the turning planes at different frequencies in different locations inside the crystal.

In order to analyze the sound enhancement and its properties, we analyze the cases of three frequencies, 2450, 2700 and 2900 Hz. Figures 4(c)-4(e) show the axial distributions of the normalized intensity,  $|I|/|I_0| = |p|^2/|p_0|^2$ , obtained experimentally (dots) and theoretically (continuous lines) for these three frequencies respectively. In both cases, small-scale fringes are observed, corresponding to the local Bloch mode, as well as a large-scale oscillations or envelope (dashed line) of the Bloch mode, as it is previously analyzed in Section III. On the other hand, at the same frequencies, the maximal sound enhancement are placed at  $x = 43.18$  cm,  $50.48$  cm and  $57.68$  cm respectively as it can be seen in Figs. 4(c)-4(d). Therefore, in correspondence with the results shown in Fig. 2 from our coupled mode theory, the position of the bright plane (corresponding to the sound enhancement) for every case is shifted back with respect to the turning plane. Moreover, the position of the maximal sound enhancement shifts deeper into the bulk of the structure as the frequency is increased, which is a clear sign of the acoustic rainbow effect produced by this kind of structures.

We pay attention now to the maximum value of the wave enhancement. Since the plots are normalized with respect to the incident wave, we can see that at the maximum value of wave enhancement, the intensity is around 60 times higher than that of the incident one. This result

improves the previously obtained for a linear chirped crystal,<sup>20</sup> which produces an enhancement of 20. We notice here that for usual reflection between two different homogeneous media or from a purely band-gap material in the range of the band-gap, only an increase of 4 times of the local intensity is possible.

The envelopes shown in Figs. 4(c)-(e) with red dashed lines, connect the experimental and numerical results with those obtained with our model based on coupled mode theory. As we previously described in Fig. 2 this red dashed lines correspond to the envelopes of the Bloch modes and they are not due to conditions imposed at the entrance of the sonic crystal as for example some possible impedance mismatch.

## VI. TIME SPREADING

In this part we analyze the effects of chirped lattice constant on the wave propagation evaluated in time domain, i.e. the effects on the character of the time spreading of the pulse reflected from the chirped structure. For that purpose, FEM simulations in time domain were carried out for the three frequencies previously mentioned, 2450, 2700 and 2900 Hz. For the simulations we use a gaussian pulse centered at these frequencies with fixed bandwidth  $\Delta\omega = 100$  Hz. During the simulations we consider here that the gaussian beam propagates from left to right.

Figure 5 shows the time-space scenario for  $f = 2700$  Hz, where the sound pressure amplitude,  $p$ , is shown. Figure 5(a) shows the pulse propagating in air and reflecting from a rigid wall placed at the position corresponding to the turning plane of the chirped structure for this specific frequency. As expected, the relation between  $x$  and  $t$  is a straight line and its slope is given by the sound velocity in air. The amplitude is modulated in  $x$  due to the interference between the incident and reflected wave.

Figure 5(b) shows the pulse propagating in air from  $x = [0, 1]$  m, and along the chirped structure (placed in the range  $x = [1, 2]$  m). The effect of soft reflection is clearly observed here. The incident wave is reflected first at the turning plane corresponding for the central frequency, around  $x = 1.6$  m, producing the bright plane just a bit before due to the reduction of the group velocity (as shown in previous Sections). After this first reflection, the pulse travels back out of the structure. In contrast to the rigid wall case, the wave here is reflected back and forth between the entrance and the turning planes of the chirped structure, giving rise to multiple contributions propagating back.

Time profiles of the signals are shown in Figs. 5(c) and 5(d) evaluated at the positions marked by the green vertical lines in Figs. 5 (a) and (b). Whereas the recorded signal for the case of a rigid wall is the superposition of incident and reflected waves with a determined duration, the recorded signal

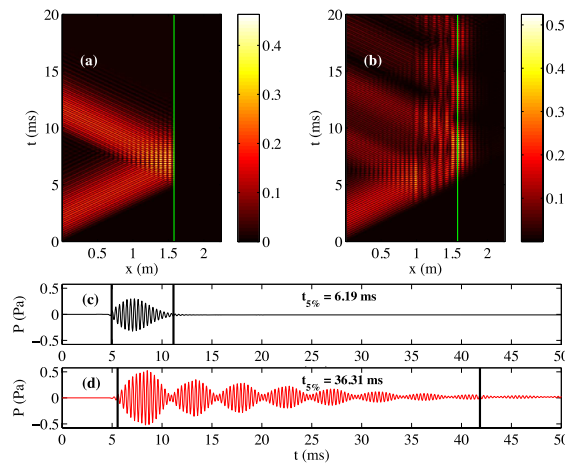


FIG. 5. Figure accounting for the time spreading of the input signal in the chirped sonic crystal. (a), (b) show the time signals recorded for a longitudinal cut in  $x$  direction, for an homogeneous medium (air), and the exponential chirped structure placed in the range  $x = [1, 2]$  m, respectively. A rigid wall is placed in  $x = 1.765$  m for the homogeneous case. Green solid lines indicate the position of the time signals shown in (c), (d). Recorded time signals for (c) an homogeneous medium and (d) exponential chirped structure, at  $x = 1.505$  m.



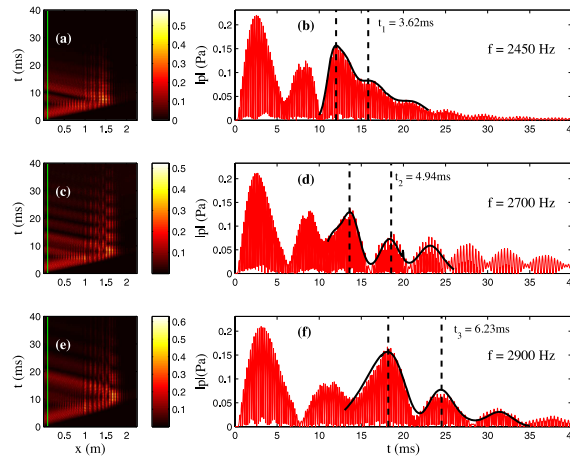


FIG. 6. (a), (c) and (e) Show the time-space maps for 2450, 2700 and 2900 Hz, and (b), (d), (f) the time profiles evaluated at  $x = 0.1$  m. The amplitude for every inset is given by the absolute value of the pressure,  $|p|$ . Green lines shown in (a), (c), (e) illustrate the corresponding positions of the bright planes for the frequencies 2450, 2700 and 2900 Hz, respectively. Black solid lines in insets (b), (d), (f), represent the fitted Gaussian functions used to estimate the delay between consecutive contributions, which are  $t_1 = 3.62$ ,  $t_2 = 4.94$  and  $t_3 = 6.23$  ms, for 2450, 2700 and 2900 Hz, respectively.

for the chirped structure has a longer duration due to the slowing down of the group velocity and it is modulated by the several contributions due to multiple reflections back and forth of the wave inside the chirped crystal. The duration of the whole signal is determined using the criteria that the duration is the time between the instants at which the amplitude is a 5 % of the maximum amplitude of the pulse. This instants are marked in Figs. 5(c) and 5(d) by vertical lines. With this criteria, the time duration of the pulse for the reflection in a rigid wall is 14.5 ms (see Fig. 5(c)), while the duration of the pulse in the chirped crystal is 40.5 ms (see Fig. 5(d)). A similar phenomenon of pulse spreading is reported in Ref. 31, where sound diffusers based on biperiodic sonic crystal structures are presented.

Time-space maps for 2450, 2700 and 2900 Hz and time profiles evaluated at  $x = 0.1$  m are represented in Fig. 6. As it was previously mentioned, several contributions appear in the upper part of every map  $x$ - $t$  corresponding to the successive reflections of the wave packet inside the chirped structure. The wave packet, as it propagates inside the structure, is slowed down and reflected in the turning plane, propagating back to the entrance, but also reflected again in the entrance. This process is repeated until the amplitude of the wave is vanished. This modulation effect by reflections is clearly shown in the signals recorded at  $x = 0.1$  m, shown in Figs. 6(b), (d), and (f), where the amplitude is given by the absolute value of the sound pressure,  $|p|$ . From the time delay between two different reflections, as we will see immediately, we can obtain information about the slowing down in the crystal. To evaluate this delay between two consecutive reflections from the numerical time domain simulations, time signals are fitted using gaussian functions.<sup>32</sup> Calculating the distance between the two centroid marked in the same Figs. 6(b), (d) and (f), these values are 3.6, 4.9 and 6.2 ms.

This delay is related to the acoustic path of the pulse inside the chirped structure in which the group velocity gradually changes. Following our approach we can calculate the value of the group velocity in every plane of the structure at each frequency using the corresponding band structures ( $v_g = \partial\omega/\partial k$ , Fig. 1), i.e., we are able to evaluate the group velocity profile inside the structure. Table I shows the group velocity values for the three frequencies evaluated in this Section. Taking into account these values and the position of the turning plane for every frequency, we can calculate the delay between two consecutive reflections of the pulse simply by the following expression

$$t_f^{\text{delay}} := 2 \int \frac{dx}{v_f(x)} = 2 \sum_{i=1}^{N_f} \frac{a_i}{v_{f,i}}. \quad (5)$$

where the integral has been replaced by a sum considering that the velocity is kept constant and equal to the value deduced from the band structures that corresponds to the lattice constant  $a_i$  for

TABLE I. Values of the group velocity deduced from the band structures calculated with Plane Wave Expansion, for every frequency analyzed and for the different values of the lattice constant  $a$ , associated to every plane of the chirped structure.

Lattice constant $a$ (cm)	$v_g$ (ms <sup>-1</sup> )		
	2450 Hz	2700 Hz	2900 Hz
12,50	254.92	94.24	89.75
11,03	292.86	278.36	52.91
9,87	296.37	296.37	284.52
8,95	276.88	287.53	292.49
8,18	196.34	265.07	274.88
7,54	0	154.80	245.86
6,99	0	0	83.77
6,52	0	0	0

every crystal plane. The time delay depend on frequency, as it is explicitly indicated in the summation.  $N_f$  depends on  $f$  because this sum extends up to the turning plane which depends on the frequency  $f$ , because of the chirped. The values obtained applying Eq. (5) are respectively 3.9, 6.3 and 11.1 ms. Although these values are compatible with the ones obtained by the gaussian fitting of the selected peaks in Figs. 6(b), (d) and (f), some differences are found for 2700 and 2900 Hz. These can be explained considering that the difference in the group velocity between air and the first two planes of the chirped structure, according to the values shown in Table I, is very large. A wave packet travelling into a perfectly periodic structure having the lattice constant of either of the two first planes of the chirped structure,  $a = 12.5$  or  $a = 11.03$  cm, will slow down gradually till the theoretical value of the group velocity is achieved, after travelling through several planes of the structure. Hence, the same wave packet entering the chirped structure will not reach this theoretical value of the group velocity, but slow down slightly before passing the first two planes.

## VII. CONCLUSIONS

Sound enhancement in chirped crystals has been revealed as an efficient mechanism for the wave spatial localization depending on its frequency and on the parameters of the structure. The acoustic wave can be selectively enhanced at particular depth of the crystal, producing bright planes for the frequencies around the first gap along the propagation direction. We reveal here that an exponential chirp can present a stronger enhancement than that produced by a linear chirp, showing an enhancement of 60 times in intensity. A simple couple mode theory is proposed, that captures well the observed effects. For testing these ideas an experimental setup was constructed based on chirped sonic crystal in the audible regime. Measurements of the acoustic field inside of the chirped structure were obtained. On the other hand, numerical calculations using FEM in the spatial and time domain have been performed, showing a perfect agreement with the experimental results. The results and insights from our simple analytical model based on coupled modes theory allow us to keep confidence over the approaches adopted, specially the consideration of our structure as locally periodic. In addition, the reflection from chirped structures was also studied in time domain, by numerical simulations, which show a measurable time spreading of the reflected pulse. The latter result is in accordance with our concept of field slowing down and spatial localization at the turning plane of chirped crystal. Generally speaking, the effect of wave enhancement opens new possibilities for increasing the efficiency of detectors and absorbers, both in acoustics and optics, since slow phonons and photons can be absorbed and harvested with a higher probability.

## ACKNOWLEDGMENTS

The work was supported by Spanish Ministry of Economy and European Union FEDER through project FIS2011-29731-C02-02. LMGR Acknowledges Supported by MINECO and FEDER, under

Grant MTM2012-36740-c02-02. ACR is grateful for the support of Programa de Ayudas e Iniciativas de Investigación (PAID) of the UPV.

- <sup>1</sup> J. D. Joannopoulos, S. G. Johnson, J. N. Winn, and R. D. Meade, *Photonic Crystals. Molding the Flow of Light* (Princeton University press, 2008).
- <sup>2</sup> Y. Pennec, J. O. Vasseur, B. Djafari-Rouhani, L. Dobrzynski, and P. A. Deymier, *Surface Science Reports* **65**, 229 (2010).
- <sup>3</sup> M. Kushwaha, P. Halevi, L. Dobrzynski, and B. Djafari-Rouhani, *Phys. Rev. Lett.* **71**, 2022 (1993).
- <sup>4</sup> R. Martínez-Sala, J. Sancho, J. V. Sánchez, V. Gómez, J. Llinares, and F. Meseguer, *Nature* **378**, 241 (1995).
- <sup>5</sup> X. Zhang and Z. Liu, *Appl. Phys. Lett.* **85**, 341 (2004).
- <sup>6</sup> M.-H. Lu, C. Zhang, L. Feng, J. Zhao, Y.-F. Chen, Y.-W. Mao, Y.-Y. Zhu, S.-N. Zhu, and N.-B. Ming, *Nature Mat.* **6**, 744 (2007).
- <sup>7</sup> I. Pérez-Arjona, V. J. Sánchez-Morcillo, J. Redondo, V. Espinosa, and K. Staliunas, *Phys. Rev. B* **75**, 014304 (2007).
- <sup>8</sup> V. Espinosa, V. J. Sánchez-Morcillo, K. Staliunas, I. Pérez-Arjona, and J. Redondo, *Phys. Rev. B* **76**, 140302(R) (2007).
- <sup>9</sup> Y. Zhou, M.-H. Lu, L. Feng, X. Ni, Y.-F. Chen, Y.-Y. Zhu, S.-N. Zhu, and N.-B. Ming, *Phys. Rev. Lett.* **104**, 164301 (2010).
- <sup>10</sup> V. Sánchez-Morcillo, R. Picó, I. Pérez-Arjona, and K. Staliunas, *Applied Acoustics* **73**, 302 (2012).
- <sup>11</sup> R. Picó, V. Sánchez-Morcillo, I. Pérez-Arjona, and K. Staliunas, *Appl. Acoust.* **73**, 302 (2012).
- <sup>12</sup> A. Khelif, P. A. Deymier, B. Djafari-Rouhani, J. O. Vasseur, and L. Dobrzynski, *J. Appl. Phys.* **94**, 1308 (2003).
- <sup>13</sup> F. Cervera, L. Sánchez, J. Sánchez-Pérez, R. Martínez-Sala, C. Rubio, and F. Meseguer, *Phys. Rev. Lett.* **88**, 023902 (2002).
- <sup>14</sup> A. Cebrecos, V. Romero-García, R. Picó, I. Pérez-Arjona, V. Espinosa, V. Sánchez-Morcillo, and K. Staliunas, *J. Appl. Phys.* **111**, 104910 (2012).
- <sup>15</sup> X. Li, X. Ni, L. Feng, M. Lu, C. He, and Y. Chen, *Phys. Rev. Lett.* **106**, 084301 (2011).
- <sup>16</sup> V. Romero-García, J. Sánchez-Pérez, S. Castiñeira Ibáñez, and L. Garcia-Raffi, *Appl. Phys. Lett.* **96**, 124102 (2010).
- <sup>17</sup> V. Romero-García, J. Sánchez-Pérez, and L. Garcia-Raffi, *J. Appl. Phys.* **108**, 044907 (2010).
- <sup>18</sup> H. Hu, A. Strybulevych, J. H. Page, S. E. Skipetrov, and B. A. van Tiggelen, *Nature Physics* **4**, 945 (2008).
- <sup>19</sup> R. Sainidou, N. Stefanou, and A. Modinos, *Phys. Rev. Lett.* **94**, 205503 (2005).
- <sup>20</sup> V. Romero-García, R. Picó, A. Cebrecos, V. Sánchez-Morcillo, and K. Staliunas, *Appl. Phys. Lett.* **102**, 091906 (2013).
- <sup>21</sup> E. Cassan, C. K.-V. D. Caer, D. Marris-Morini, and L. Vivien, *J. Lightwave Tech.* **29**, 1937 (2011).
- <sup>22</sup> Y. Cheng, S. Kicas, J. Trull, M. Peckus, C. Cojocar, R. Vilaseca, R. Drazdys, and K. Staliunas, *Sci. Rep.* **4**, 6326 (2014).
- <sup>23</sup> M. Kushwaha, B. Djafari-Rouhani, L. Dobrzynski, and J. Vasseur, *Eur. Phys. J. B* **3**, 155 (1998).
- <sup>24</sup> I. E. Psarobas and M. M. Sigalas, *Phys. Rev. B* **66**, 052302 (2002).
- <sup>25</sup> L. Wu and L. Chen, *J. Appl. Phys.* **110**, 114507 (2011).
- <sup>26</sup> Y. Shen, J. Fu, and G. Yu, *Phys. Lett. A* **375**, 3801 (2011).
- <sup>27</sup> M. Stockman, *Phys. Rev. Lett.* **93**, 137404 (2004).
- <sup>28</sup> V. N. Smolyaninova, I. I. Smolyaninov, A. V. Kildishev, and V. M. Shalaev, *Appl. Phys. Lett.* **96**, 211121 (2010).
- <sup>29</sup> E. Centeno, D. Cassagne, and J.-P. Albert, *Phys. Rev. B* **73**, 235119 (2006).
- <sup>30</sup> <http://functions.wolfram.com/HypergeometricFunctions/LaguerreL3General/>.
- <sup>31</sup> J. Redondo, R. Picó, V. J. Sánchez-Morcillo, and W. Woszczyk, *J. Acoust. Soc. Am.* **134**, 4412 (2013).
- <sup>32</sup> A. Cicek, O. A. Kaya, M. Yilmaz, and B. Ulug, *J. Appl. Phys.* **111**, 013522 (2012).